Geophysical Journal International

Geophys. J. Int. (2012) **188,** 103–114 doi: 10.1111/j.1365-246X.2011.05259.x

Multiscale analysis of potential fields by a ridge consistency criterion: the reconstruction of the Bishop basement

M. Fedi,[1] G. Florio[1] and L. Cascone[2]

[1] *Department of Earth Sciences, University of Naples 'Federico II', Naples, Italy. E-mail: gflorio@unina.it*
[2] *GETECH, Leeds, UK*

Accepted 2011 October 4. Received 2011 October 4; in original form 2010 November 30

SUMMARY

We use a multiscale approach as a semi-automated interpreting tool of potential fields. The depth to the source and the structural index are estimated in two steps: first the depth to the source, as the intersection of the field ridges (lines built joining the extrema of the field at various altitudes) and secondly, the structural index by the scale function. We introduce a new criterion, called 'ridge consistency' in this strategy. The criterion is based on the principle that the structural index estimations on all the ridges converging towards the same source should be consistent. If these estimates are significantly different, field differentiation is used to lessen the interference effects from nearby sources or regional fields, to obtain a consistent set of estimates. In our multiscale framework, vertical differentiation is naturally joint to the low-pass filtering properties of the upward continuation, so is a stable process. Before applying our criterion, we studied carefully the errors on upward continuation caused by the finite size of the survey area. To this end, we analysed the complex magnetic synthetic case, known as Bishop model, and evaluated the best extrapolation algorithm and the optimal width of the area extension, needed to obtain accurate upward continuation. Afterwards, we applied the method to the depth estimation of the whole Bishop basement bathymetry. The result is a good reconstruction of the complex basement and of the shape properties of the source at the estimated points.

Key words: Gravity anomalies and Earth structure; Magnetic anomalies: modelling and interpretation.

1 INTRODUCTION

The study of gravity and magnetic fields at different altitudes, so constituting a multiscale data set, is an important part of several interpretation methods (e.g. Paul *et al*. 1966; Paul & Goodacre 1984; McGrath 1991; Pedersen 1991). More recently, other methods involving a multilevel data set were proposed, among which the continuous wavelet transform method (CWT; e.g. Mallat 1998; Sailhac & Gibert 2003), the depth from extreme points (DEXP) method (Fedi 2007) or methods using the scale function (Fedi & Florio 2006; Fedi 2007; Florio *et al*. 2009). Other multiscale methods are the Euler deconvolution of vertical profiles of potential fields (Florio & Fedi 2006) and the multiridge analysis with reduced Euler deconvolution (Fedi *et al*. 2009; Florio & Fedi 2009).

Interpretation of potential fields by these methods is based on the recognition that the gravity or magnetic effect, $f(x)$, generated by ideal sources (point mass, line of mass, sheet and contact) is a homogeneous function,

$$f(tx) = t^n f(x), \tag{1}$$

where n is the homogeneity degree and t is the homogeneity coefficient. Although t could be arbitrarily chosen (Stavrev & Reid 2007), the exponent n changes with the source type and it is integer and constant for the ideal sources, whereas it is fractional and varies within the harmonic region for complex sources (Steenland 1968).

By multiscale methods, the depth to the source of homogeneous fields can be determined by a geometric approach: as a consequence of the dilation of potential fields versus the altitude, the maxima of the field modulus at various scales are located along straight lines ('ridges'). In the case of homogeneous potential fields, sources are located at singular points of the field, under the measurement level. According to Moreau *et al*. (1997), the source depth could be recovered by simply extrapolating the ridges below the measurement surface and by identifying their intersection point (Fig. 1).

The structural index is the opposite of the homogeneity degree ($N = -n$). It characterizes the shape of simple sources generating homogeneous fields. Simple sources, such as spheres, horizontal cylinders and sills, have singular points corresponding to their centre; for dykes, vertical cylinders and contacts, the singular point corresponds to the top of the source. The estimation of the source structural index is an important step in potential field interpretation and it is particularly well suited using multiscale methods.

Multiscale methods need the field to be known at many altitudes. However, direct measurement of the field at many altitudes is

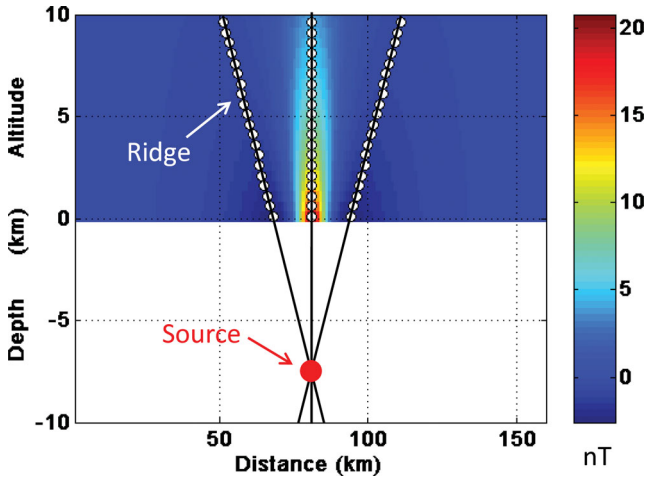

Figure 1. The geometrical method to retrieve the source depth and horizontal position. Ridges, defined by the position of the extrema of the potential field at several altitudes, develop as straight lines for simple sources and intersect below the measurement plane at the source position.

currently not feasible. For this reason, this class of methods uses the upward-continuation algorithm to create a 3-D data set. This well-known transformation of potential fields is based on the equation (e.g. Gibert & Galdéano 1985)

$$G(x,y,z) = \frac{1}{2\pi}\iint_S G(\xi,\eta,z_m) \times \frac{z-z_m}{\left[(x-\xi)^2+(y-\eta)^2+(z-z_m)^2\right]^{3/2}}\,\mathrm{d}\xi\,\mathrm{d}\eta, \quad (2)$$

where $G(x, y, z_m)$ is the measured potential field at z_m, $z < z_m$ is the altitude of continuation and S is an infinitely extended region, where the field should be measured continuously, in principle. This equation is a convolution integral and relates linearly the data at some level z_m to those at highest levels in the harmonic region. Upward continuation is a well-known stable filter, and this stability with respect to the noise is, therefore, shared also by multiscale methods (e.g. Fedi *et al*. 2009).

Anyway, to use the above methods, some care must be taken in order that the application of eq. (2) to a finite and discrete set of potential field data, known on a finite region, could yield accurate results. The most severe errors commonly arise when using conventional circular convolution fast Fourier transform (FFT) algorithms, because frequency aliasing errors can affect the low-frequency content of the upward-continued data at high altitudes. Fortunately, these errors can be kept low by performing the circular convolution on a larger area than that of interest (Oppenheim & Schafer 1975). Therefore, the input data sequences can be extended to a greater length by using other surveys in nearby areas, if available, or, alternatively, by mathematical extrapolation algorithms, such as zero-padding, maximum entropy prediction, symmetrization and others.

In this paper, we propose a two-step multiscale method to obtain depth and structural index from the analysis of the gravity or magnetic field.

The first step for using multiscale methods is the generation of a 3-D data set by using the upward-continuation algorithm. For this reason, in the first part of the paper, we are interested in the evaluation of the errors related to the upward-continuation process. This will be done by comparing the magnetic field of the central part of the Bishop model upward continued to 10 km (after being enlarged by various extrapolation algorithms) with the theoretical magnetic field of the Bishop model generated at the same 10 km altitude.

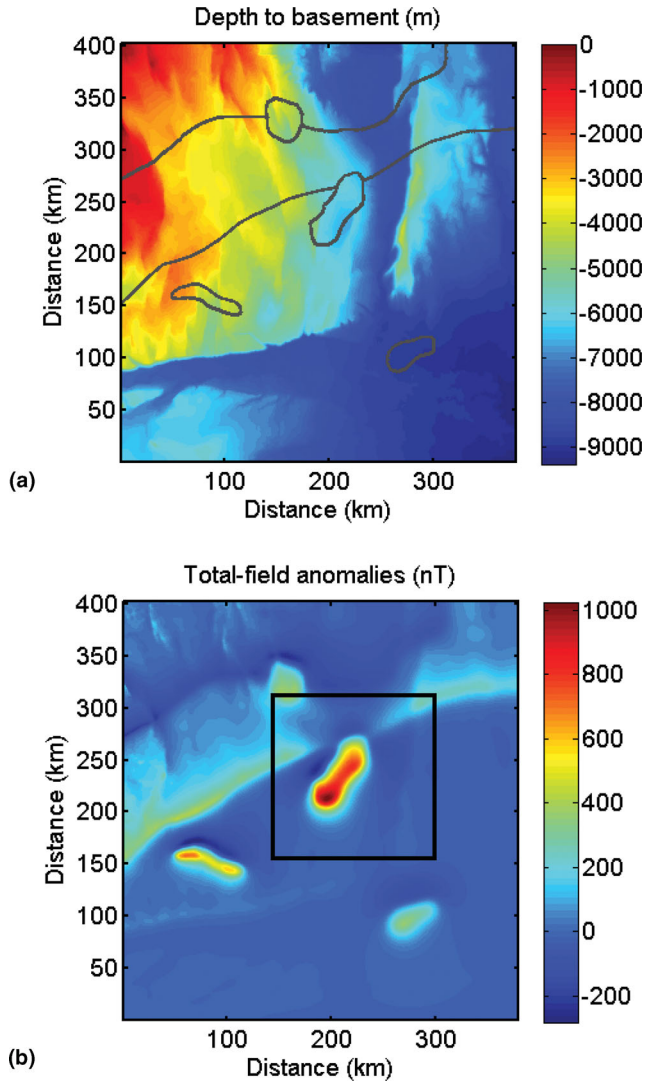

Figure 2. Bishop synthetic basement model. (a) Map of the depth to basement. Grey lines mark the vertical susceptibility discontinuities. (b) Bishop model total-field anomalies computed at sea level and with a geomagnetic field inclination of 60°.

As a second step, we will use the ScalFun method to estimate the structural index N for each analysed ridge. ScalFun is a multiscale approach proposed by Fedi & Florio (2006) and Fedi (2007), who analysed potential fields at several scales with the scale function τ_m, which is defined as

$$\tau_m = \frac{\partial \log f_m}{\partial \log z} = -N_s \frac{z}{z-z_0}, \quad (3)$$

where N_s is the structural index relative to the field f_m, $m = 3$ in the magnetic case and $s = m$–3, so that N_0 is the structural index for the magnetic field. The scale function is, therefore, a function of the depth to source z_0, of N_s and of the altitude z.

A magnetic anomaly data set generated by a synthetic complex model of magnetic basement, known as the Bishop model (Williams *et al*. 2002), will be used to test the performance of the method when

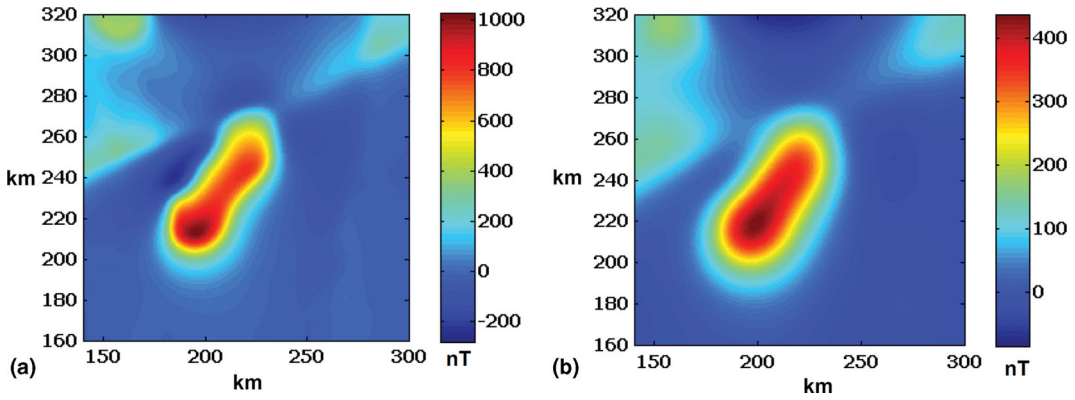

Figure 3. (a) Details of the Bishop model total-field and (b) its upward continuation to 10 km.

applied to a realistic source model. It will be also possible to assess the best strategy in data extrapolation to perform a correct upward continuation of potential fields.

The so-called 'Bishop model' represents a magnetized basement model. The real topography data of the volcanic tablelands, north of Bishop (CA), have been used as the surface of a magnetic basement, overlain by non-magnetic sediments. The area was chosen because it contains a variety of structures: two relatively long, large-offset faults, en echelon arrays of smaller scale north–south faults, transfer zones between faults and an unfaulted deep-basin area in the southeast corner (Fig. 2). Susceptibility boundaries (lithological changes or intrusive bodies) and a Moho at a variable depth were added to complicate the magnetic model (Williams *et al*. 2005). Other authors, besides the inventors of the model, used the synthetic magnetic anomalies generated by this model to test depth and shape source-estimators techniques (e.g. Reid *et al*. 2005; Goussev & Pierce 2010).

In Section 3, we will describe the ScalFun method and will introduce a 'consistency criterion' to improve the accuracy and to assess the reliability of the solutions. Finally, in Section 4, we use this analysis to recover the depth to the magnetic basement of the Bishop model, and to obtain also information about the source types originating the anomalies.

2 REDUCING ERRORS ON UPWARD-CONTINUED DATA

To reduce upward-continuation errors when conventional circular convolution FFT algorithms are used and, thus, to create a reliable 3-D data set for multiscale analysis, we tested several methods to extrapolate on a bigger area the field to be upward continued.

Our tests were performed on the magnetic field of the Bishop model, computed at sea level and with a geomagnetic field inclination of 60° and a declination of 0° (Fig. 2b). The data-sampling step of the model is 0.2 km and we upward continued the sea level data set from 0 to 10 km altitude, that is, up to 50 times the sampling step (Fig. 3b). To estimate the error related to the upward-continuation process, we used the field of the Bishop model computed directly at 5 and 10 km altitudes.

To consider a more realistic scenario, we extracted a central area of 800 × 800-cell grid size of the ground data. It can be seen in Fig. 3 that the northern and western edges of such a subarea cut some high-amplitude anomalies. In this situation, similar to a real-world case, upward-continuation errors may be induced in the continued field.

As already said, to reduce errors near the boundaries, a data set based on an area larger than the measurement area should be used. In many cases, real data outside the region of interest are not available, so the data set must be extrapolated by using suitable algorithms.

In our test, we estimated the misfit between the theoretical field at 10 km and the upward-continued data enlarged by using either ordinary extrapolation algorithms, such as zero-padding and periodized extension, or more unconventional ones, such as the maximum entropy extension. Other algorithms may also be used, but we stop our analysis to the following seven methods for practical reasons:

1. *Maximum entropy extension algorithm (Gibert & Galdéano 1985):* the method is based on the extrapolation with a predictive filter derived from Burg's maximum entropy spectral analysis algorithm (Fig. 4a).
2. *Smooth extension of order 0:* this method implements a simple constant extrapolation outside the original support. For a 1-D signal, the extension is the repetition of the first value on the left-hand size and last value on the right-hand size (Fig. 4b).
3. *Smooth extension of order 1:* this method implements a simple first-order derivative extrapolation, padding using a linear extension fit to the first two and last two values. The smooth padding methods work well in general for smooth signals (Fig. 4d).
4. *Symmetric extension:* this method assumes that signals can be recovered outside their original support by symmetric boundary-value replication (Fig. 4c).
5. *Antisymmetric extension:* this method uses an antisymmetric boundary-value replication outside their original support. Symmetric and antisymmetric extensions have the disadvantage of creating artificial discontinuities of the first derivative at the edge (Fig. 4e).
6. *Periodized extension:* this method uses a periodic extension extrapolation algorithm outside the original support. The disadvantage of periodic padding is that discontinuities are artificially created at the edges, especially on truncated anomalies (Fig. 4f).
7. *Zero padding:* this method extrapolates with zeros the original support. The disadvantage of zero padding is that, discontinuities are artificially created at the edges. This effect can be reduced extrapolating with the field average value instead, than with zero.

For each of the above methods, we made several tests changing the extent of the extrapolated data, varying from 25 per cent up to 150 per cent of the original data size (Fig. 3).

The smallest error was obtained by using the maximum entropy extension algorithm (Fig. 4a). As expected, the greatest errors are concentrated mainly along the western and northern edges, in correspondence with incomplete and intense anomalies (Fig. 5). The

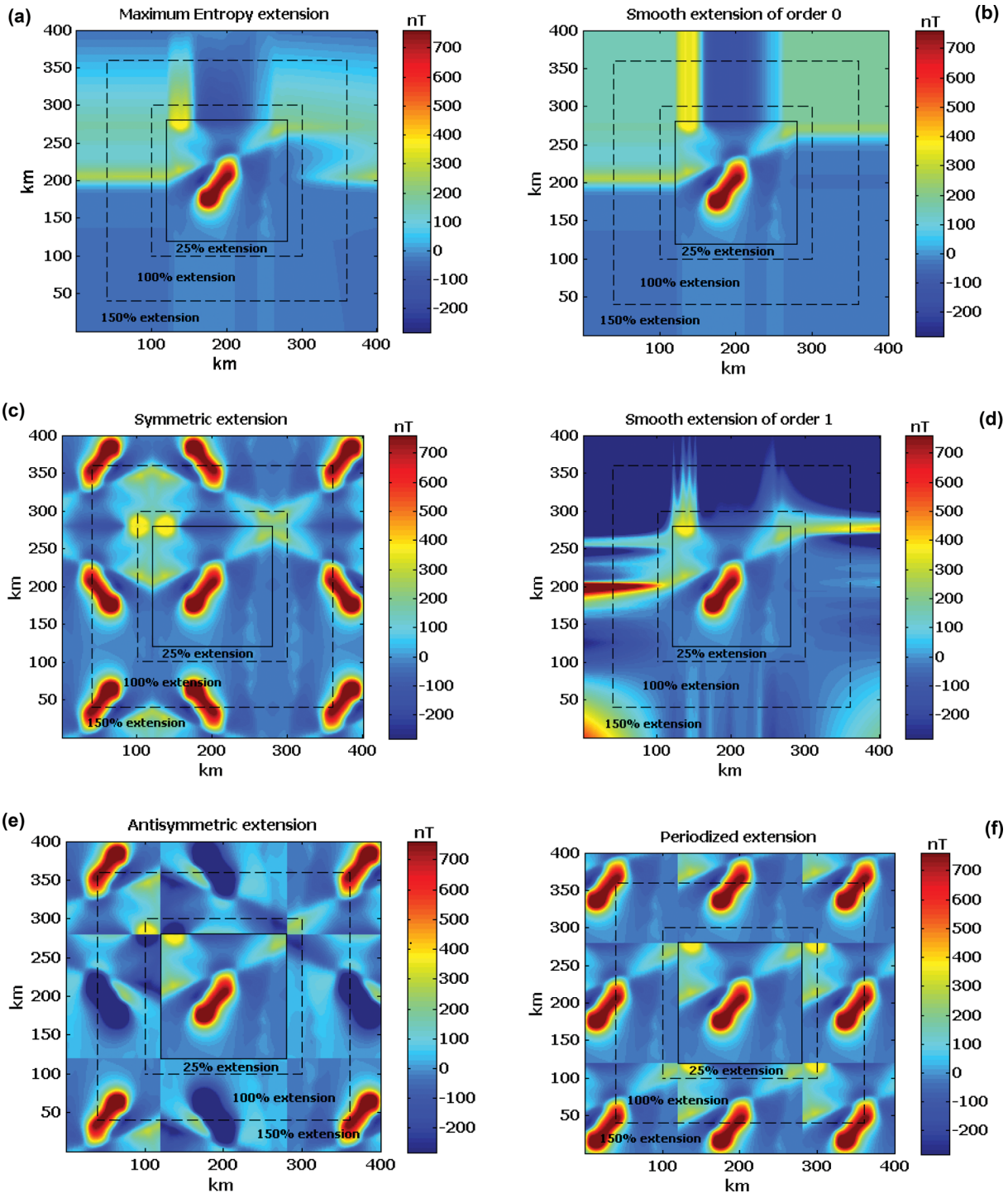

Figure 4. Examples of different extrapolation algorithms. (a) Maximum entropy extension algorithm; (b) smooth extension of order 0; (c) smooth extension of order 1; (d) symmetric extension; (e) antisymmetric extension; (f) periodized extension and (g) zero padding.

difference between the data of the model at 10 km and the upward-continued data by using the maximum entropy extension algorithm (Fig. 5a) reveals that, in the selected window, a wide central part is affected by an error close to 5 nT. The theoretical field at 10 km varies between −76 and 437 nT in the data window, so the error results to be <1 per cent. By increasing the width of the extrapolated region, the average error in the central area reduces even more (Figs 5b and c). Similar results are obtained using the 'smooth extension of order 0' algorithm (Figs 5d–f). Other algorithms perform similarly in the central area, with errors always <5 nT, but show bigger errors near the edges. Using the smooth extension of order 1 and an extension width of 25 per cent (Fig. 5g), the errors in the central area are still reduced (<3 nT), but enlarging the extension width, an almost constant-value results added to the continued anomalies (Figs 5h and i). This may be expected because when the extrapolated area is similar in size or bigger than the data area, the extrapolated data tend to be as important as the true data, and this fact may be the cause of errors at low wavenumbers.

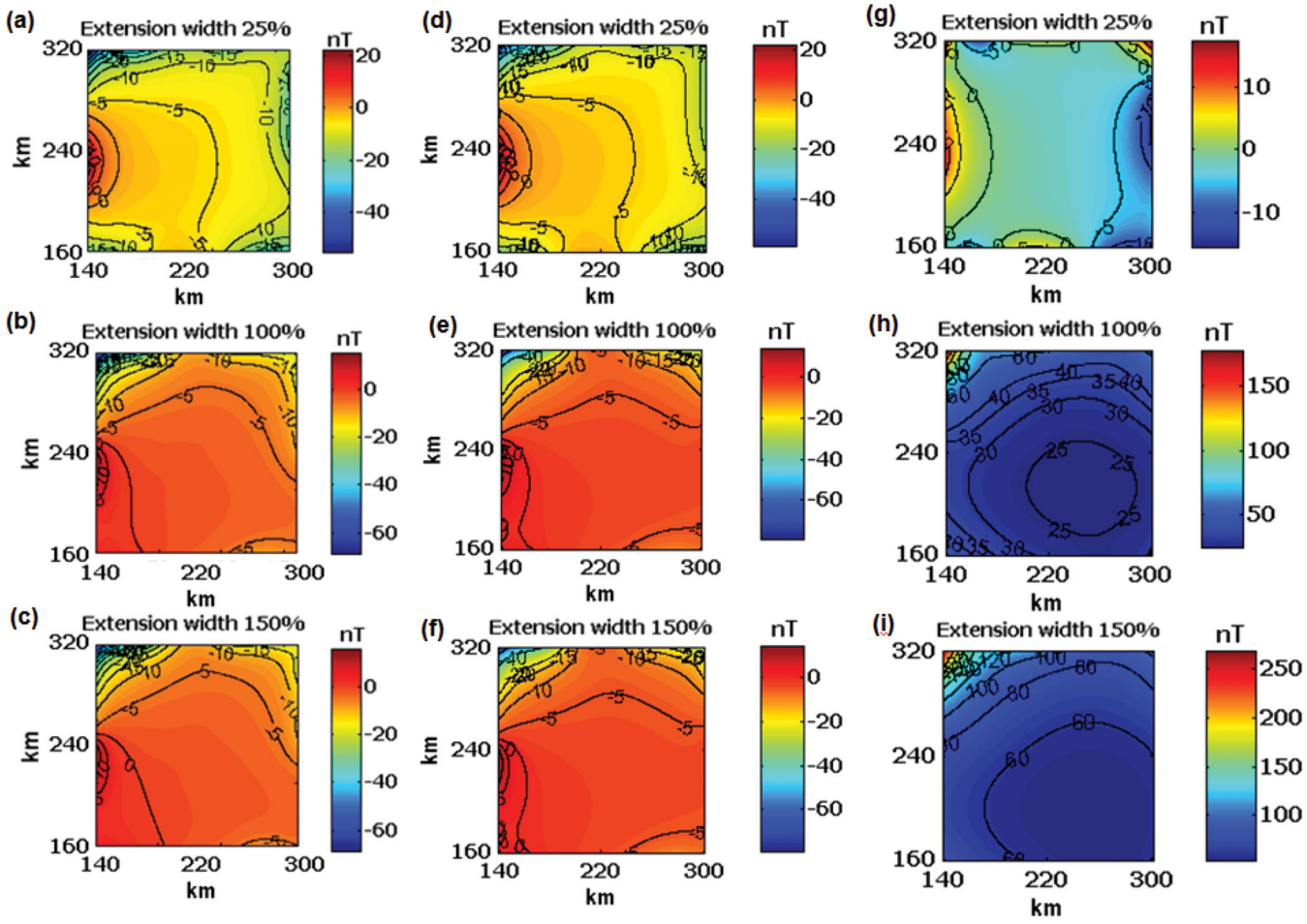

Figure 5. Difference between the data of the model computed at 10 km and the upward-continued data by using (a)–(c) maximum entropy, (d)–(f) smooth extension of order 0 and (g)–(i) smooth extension of order 1 algorithms. For each of the above methods, tests were made by changing the extent of the extrapolated data, varying from 25 to 150 per cent of the original data size.

In summary, as expected, we find that the error increases, especially, when an intense, incomplete anomaly is present at the edges and a derivative-based extrapolation algorithm is used.

It is clear that the errors produced by the upward-continuation process increase with the altitude difference as well as with the high-wavenumber content (in turn dependent on the altitude of acquisition) of the data to be continued. This means that the upward continuation from 5 to 10 km of the same Bishop data set will give more accurate results than the continuation from 0 to 10 km. In our case, we obtained significantly reduced errors by continuing the data from 5 to 10 km. The smooth extension of order 0 and 1 (Fig. 6) was used, with the extension area sized as the original data (100 per cent width). Both the extension algorithms have good performances, with the error in the central area <5 nT. This result confirms that the error in upward continuation increases with the continuation altitude and suggests that measuring data at two levels may be exploited to improve the upward-continuation quality, allowing for continuation by smaller altitude intervals. Sometimes, two magnetic or gravity data sets acquired at different altitudes, on the same area, may be available, for example, when aeromagnetic data are measured in an area when ground or marine data are already available. So, if two data sets at different altitudes are available and have a comparable data density and quality, both have to be used to obtain more accurate upward-continued data, especially if large altitude differences are needed. This point is clearly very important for any multiscale method.

3 THEORY AND METHOD

3.1 The multiscale geometrical method

As already said, homogeneous potential fields, in absence of strong noise or interference effects, develop their extrema (maximum or minimum) at several altitudes along straight lines (e.g. Fedi *et al*. 2009), due to their dilation law with distance. Such straight lines are called ‘ridges’ and intersect at the source position (Fig. 1). Thus, the geometrical method simply consists of retrieving the source position by extrapolating the ridges under the measurements plane and by considering their intersection point as the source position.

Generally, gravity or magnetic anomalies may not be sufficiently isolated, especially when measured from high altitudes. A possible choice is, hence, to improve the resolution by differentiating the field. An increased resolution is obviously expected to warrant a better depth estimation. It is well known, in fact, that the differentiated anomalies will reduce their horizontal extension because of the increased fall-off rate of the transformed field. Although every directional derivative could be used, we prefer to use the vertical

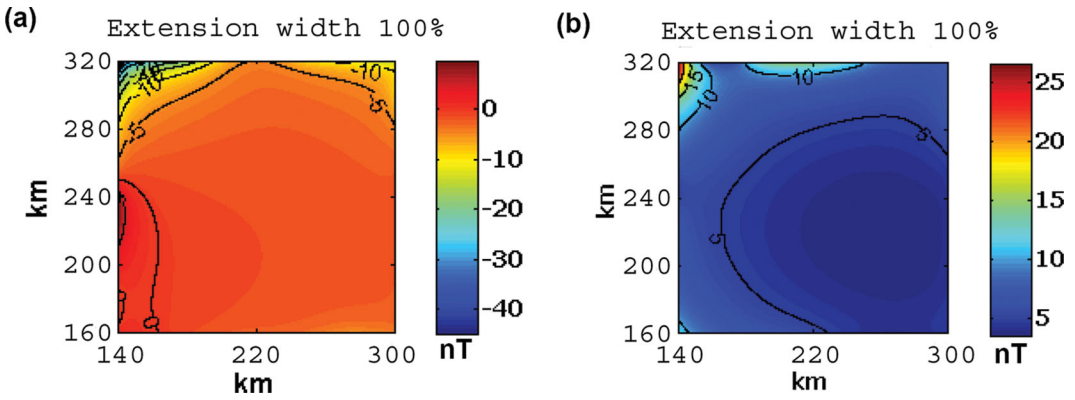

Figure 6. Difference between the data of the model computed at 10 km and the upward-continued data from 5 to 10 km by using (a) smooth extension of order 0 and (b) smooth extension of order 1 algorithms. The extent of the extrapolated data was equal in size to the dimension of the original data window.

differentiation because of its property to have no phase distortion, thus, simplifying the quality control of the whole process. Fig. 7 shows the case of interfering anomalies generated by two dipolar sources at 6 km depth. Due to their mutual interference, their ridges are not fully developed, preventing a correct application of the geometrical method. By differentiating the field, it is possible to reduce the reciprocal interference and, thus, better isolate the anomalies and obtain well-developed ridges. In real cases, the decreasing of the signal-to-noise ratio implied by the use of vertically differentiated data has to be taken into consideration. However, the upward continuation, acting as a low-pass filter, makes the differentiated field more stable. In fact, the combination of the continuation and differentiation operators can act as a bandpass filter (Fedi *et al*. 2009).

In this paper, we apply the geometrical approach, as described earlier, to the Bishop model data, to recover the basement depth.

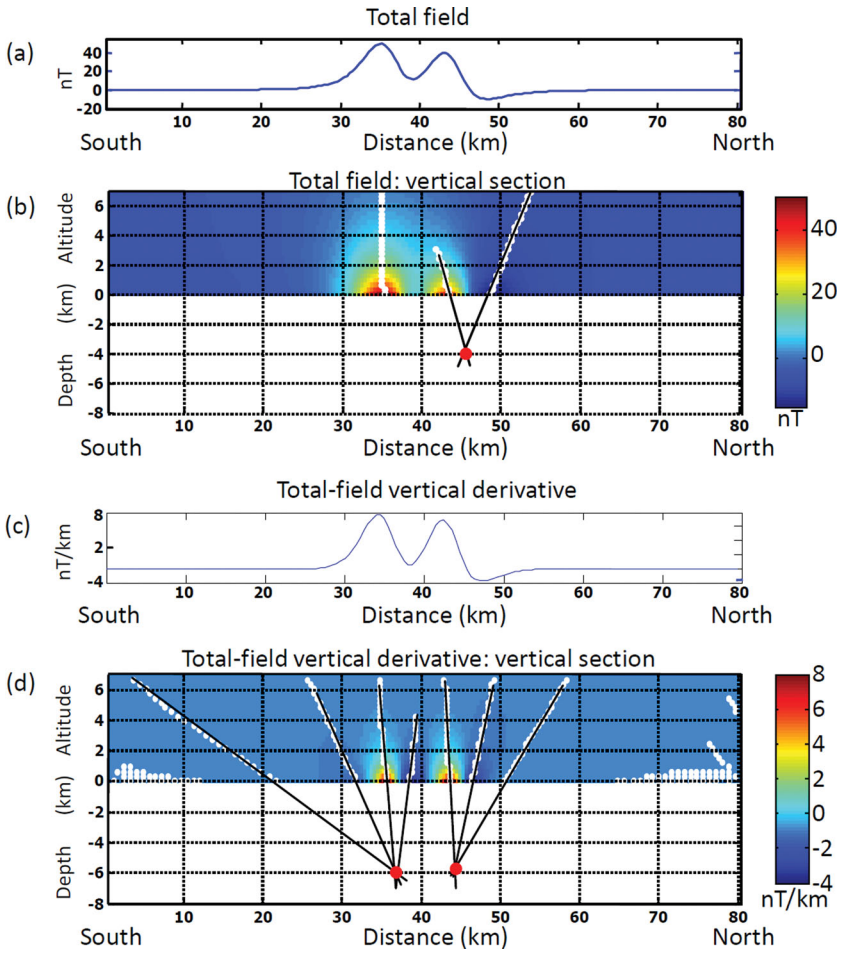

Figure 7. (a) Interfering anomalies generated by two dipolar sources at 6 km depth. (b) Interference prevents a clear development of the two sources' ridges and, thus, the geometrical method cannot be used. (c) Vertical derivative of the total field in (a). (d) By vertically differentiating the field, it is possible to reduce the reciprocal interference and, thus, better isolate the anomalies and obtain well developed ridges.

Our 3-D data set is obtained through upward continuation, using the maximum entropy edge extrapolation. To evaluate how the numerical errors produced by upward continuation could affect the depth and structural index estimates, our aim was at simulating realistic conditions. To this end, we extended the data by the approach outlined in Section 2, so renouncing to enlarge the data set with the available true synthetic data. To speed up the computations, we divided the model in 18 subareas, whose data set were each one enlarged and upward continued. Our approach to the interpretation of the Bishop basement data consists of obtaining depth estimates by the geometrical method and independent estimates of the structural index by the ScalFun method (Fedi & Florio 2006; Florio *et al*. 2009) that will be outlined in the next section. Results will be analysed and validated by the Ridge consistency criterion that we describe in Section 3.3.

3.2 ScalFun method for the structural index estimation

The ScalFun method is based on the concept of the scale function of potential fields τ, which was introduced by Fedi & Florio (2006) and Fedi (2007), to estimate the structural index, N, and the depth to source, z_0. By this method, it is possible to obtain independent estimates of N or of z_0, and also simultaneous estimates of both N and z_0.

Starting from eq. (3), we define the scale function τ_m as

$$\tau_m = -N_s \frac{z}{z - z_0}. \tag{4}$$

Note now that the origin of the z-axis is arbitrarily chosen, so the altitudes, z, and the depth to source, z_0, may be rescaled as, respectively, $z - \hat{z}_0$ and $z_0 - \hat{z}_0$, for any given depth guess, $\hat{z}_0$ (Florio *et al*. 2009)

$$\tau_m(z, \hat{z}_0) = -N_s \frac{z - \hat{z}_0}{z - z_0} \tag{5}$$

Moreover, putting $z = 1/q$, eq. (5) becomes,

$$\tau_m(q, \hat{z}_0) = -N_s \frac{1 - \hat{z}_0 q}{1 - z_0 q}, \tag{6}$$

which will be an increasing, decreasing or constant function of q, respectively for $\hat{z}_0$ lower, greater or equal to the true z_0. Moreover, for any given guess $\hat{z}_0$,

$$\tau_m(q \to 0, \hat{z}_0) = -N_s, \tag{7}$$

that is, the intercept of τ_m versus q, yields an estimate of the structural index, which is independent from the depth to source. So, such an analysis of the scaling function makes it possible to recover the structural index and the depth to source, independently or jointly.

The structural index estimates, obtained by ScalFun method, are rather stable with respect to the guess depth $\hat{z}_0$. This is illustrated in Fig. 8, in the case of the magnetic field generated by a dipolar source, located at 4 km depth: the estimated N are very close to the true one ($N = 3$) for $2.5 < \hat{z}_0 < 5.5$ km.

In this work, we estimate N by the ScalFun method, using all the ridges involved in the geometrical estimation of depth, such as the three ridges, shown in Fig. 1. For each anomaly, we estimate N by eq. (7) and by setting $\hat{z}_0$ as the depth estimated by using the geometrical method. The pairs of obtained solution (depth and N) of every group of ridges concerning the same source will be discriminated according to a consistency criterion, which we will introduce in the next section.

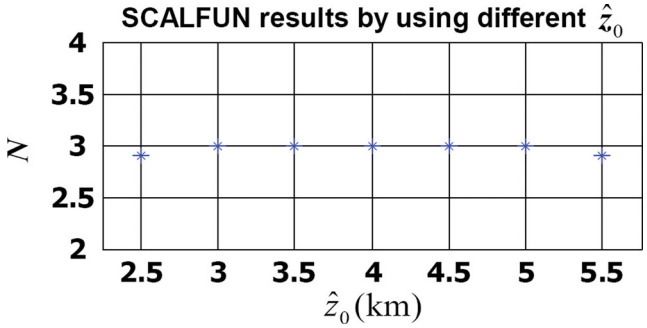

Figure 8. Stability of the structural index estimates (N) obtained with the ScalFun method with respect to the guess depth $\hat{z}_0$. The case of a dipolar source ($N = 3$) at 4 km depth is illustrated.

3.3 Ridge consistency criterion

In presence of regional fields, interference and noise, the structural index estimates obtained by the separate analysis of two or more ridges can be very different, even if they apparently converge to the same source. To discriminate the reliability of the depth solutions obtained with the geometrical method, we define a consistency criterion: it consists of evaluating the degree of closeness among the structural index estimations obtained by applying ScalFun method to the same ridges. The depth solutions are validated only if the N estimates are consistent over the considered ridges.

Field measurements may present a low signal-to-noise ratio, caused by experimental or round-off errors. It may be caused also by sampling errors, characteristic of anomalies from small/shallow geological sources, which have a so small wavelength to be not well sampled. Such errors may have a white spectrum, and affect mostly the signal-to-noise ratio at high wavenumbers. Thus, in a multiscale analysis, it is rather straightforward to account for this type of data error by simply excluding the lowest altitude data. More subtle problems to the interpretation are caused by regional fields or by interference with nearby anomalies. In the case of multiscale methods, the coalescence effects may be severely amplified at high altitudes. This kind of data contamination causes ridges to change their inclination with respect to the undisturbed case and to become curved (Fig. 9a), affecting the results obtained by the geometrical method. Field differentiation and/or exclusion of largest scales may help to fix this problem.

Thus, if the altitudes are correctly chosen following the above reasoning, ridges should be straight lines and the geometrical method should provide a correct source depth. Consistent estimates of N are also obtained for all the ridges converging towards the source. This consistency is an indication of the reliability of both the depth and structural index estimations.

On the contrary, when the interference effects are not negligible, no consistent structural index estimations are expected from the analysis of the ridges converging to the same source. The inconsistency among the solutions related to the same source provides an ambiguity in the determination of the N. In this case, even if the ridges are straight lines, the depth estimated by the geometrical method will be flawed. In these cases, to improve the consistency for our estimations, we can reduce the interference by means of a differentiation process.

As a first step, errors caused by the upward-continuation process should be minimized, as described in Section 2. Accordingly, the altitude set for the multiscale analysis should be selected as preserving the smoothing effect, while minimizing the influence of noise, as well as the edge and interference effects that affect the field at

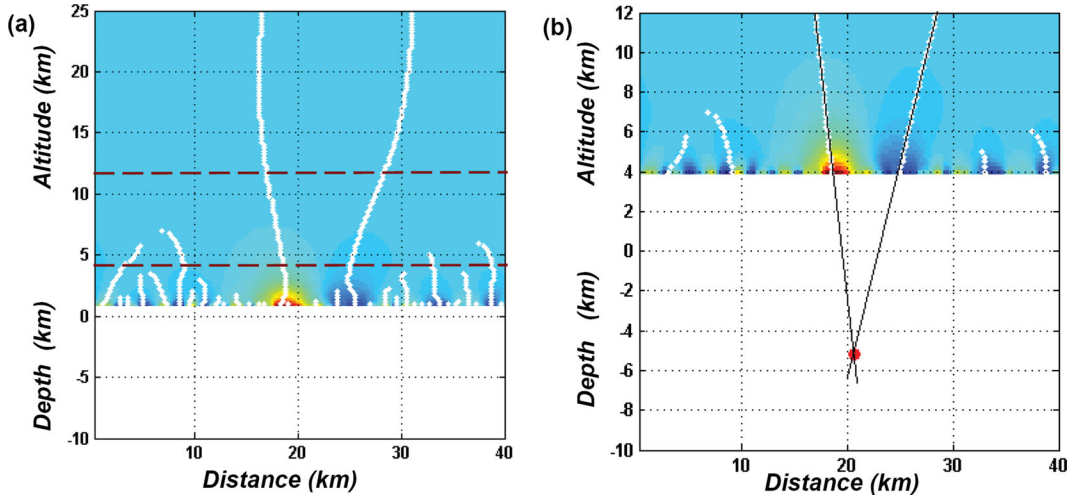

Figure 9. Choice of the altitude set for the multiscale analysis. Due to noise, interference and edge effects, linear ridges—suitable to be interpreted—are selected at altitudes between 4 and 12 km.

high altitudes, as shown in Fig. 9. The final step is to use vertical differentiation to lessen the reciprocal interference from nearby sources and, thus, to help isolating the anomalies. We remark here that the joint use of differentiation and continuation may effectively increase the anomaly separation without excessively enhancing the noise, when the combined operator is correctly tuned and assumes the shape of a bandpass filter (Fedi *et al*. 2009).

In the following section, we will use the geometrical method, for depth estimation, and the ScalFun method, for N estimation. The parameters related to the three steps outlined earlier (type of extrapolation, set of upward-continuation altitudes, order of vertical differentiation) will be varied until some consistent and reliable N estimation is reached for the ridges converging towards the same source.

We tested the ridge consistency criterion on the reduced to the pole Bishop model data, for which we achieved independent N estimations by using depths (z_0 in eq. 6) estimated by the geometrical method.

Figs 10 and 11 show an example of application of the method on one of the 18 selected windows. The red line represents the selected cross-section, along which the analysis is performed. The anomaly shown in Fig. 10(a) suffers from interference with another anomaly to the South; moreover, it is near the edge of the considered subarea and, thus, presents also a not-negligible continuation error. Fig. 10(b) shows the basement relief in the selected window. The depth to the analysed source (a magnetic contact) is 2670 m. However, because of interference effects, a strong error affects our depth estimation (Fig. 11a). The poor reliability of the depth estimates is testified by inconsistent estimates of N: from the analysis of ridge 1, we obtain $N = 2.6$, and from ridge 2, we obtain a structural index close to 0 (Figs 11b and c). Then, we turn to the second-order vertical derivative of the field, to minimize the interference effects from the nearby sources. The geometrical method gives now a much different and shallower depth estimate, and the good quality of the estimates is supported by consistent estimations of N (Figs 11d and f). We conclude that, according to our ridge consistency criterion, both solutions (depth and N) should be now accepted: the depth estimated with the geometrical method is very close to the true one (−2700 m; Fig. 11d) and also the estimated N (about 2) is consistent with the source type (magnetic

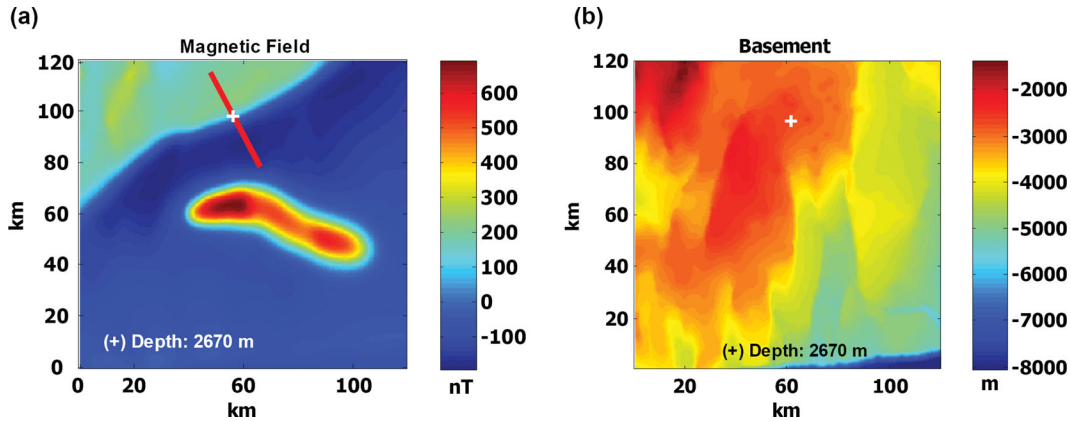

Figure 10. Example of application of the ridge consistency criterion to an anomaly of the Bishop basement. (a) Magnetic anomaly related to a lateral susceptibility contrast at 2670 m depth (white cross). The red line indicates the interpreted profile in Fig. 11. (b) Basement relief in the selected window (the white cross corresponds to the position of the magnetic contact along the selected profile).

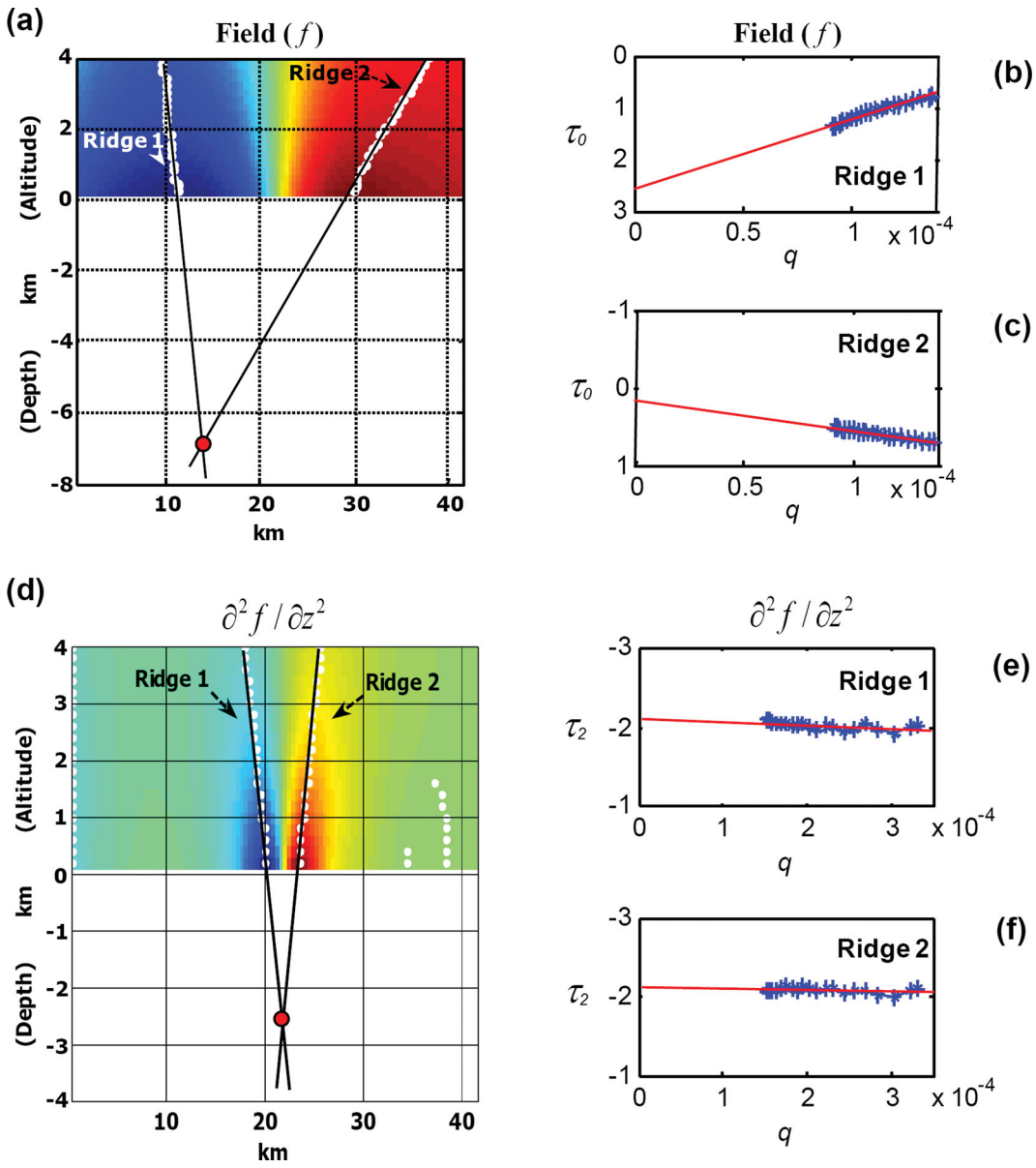

Figure 11. Interpretation of a selected anomaly from the Bishop model along a profile shown in Fig. 10. (a) The application of the geometrical method to the total field gives strong error on the depth estimation. The ScalFun method applied to the two ridges used in the geometrical method gives inconsistent estimates of N (b) and (c). (d) To minimize the effects of nearby sources, the second vertical derivative of the total field is interpreted, and the geometrical method gives a good estimation of the depth to source, supported by consistent N estimations (e) and (f). In this case the estimated N (about 2) is consistent with the source type (magnetic contact) and the analysed field (second vertical derivative of the total field).

contact) and the analysed field (second vertical derivative of the total field).

4 APPLICATION TO THE WHOLE AREA OF THE BISHOP MAGNETIC FIELD

In this section, we apply the multiscale approach, described earlier, to the Bishop model total-field map, computed with magnetic inclination of 60° and a declination of 0°, to obtain information about the basement depth so as to image the basement morpho-structural features.

Other authors have done a similar work on this data set, with different methods.

Williams *et al*. (2005) compared results obtained with 3-D Euler deconvolution with and without 2-D constraints, by which the authors can discern the source structure dimensionality and estimate the source location and depth. The Bishop model version they used, contain no susceptibility heterogeneities in the basement and the computed total field has a magnetic inclination of 45° and a declination of 0°. Williams *et al*. (2005) used a structural index, $N = 0.5$, to obtain the best results. These authors did not interpolate their results to obtain an image of the basement map, but, at the solution locations, the misfit between the estimated and the true depth is generally within 400 m and sometimes reach 2 km. Reid *et al*. (2005), by using an Euler deconvolution technique independent from the source type, obtained too few acceptable solutions to accurately reproduce the basement bathymetry. Salem *et al*. (2008), testing a method based on the tilt-angle derivatives, obtained solutions with a somewhat high vertical scatter (several kilometres). In correspondence of the main contact structures, they found solution

clusters below the basement top, as well as structural indices of about 0.5, that is, higher than the expected value associated with these source geometries.

Goussev & Pierce (2010) tested on the Bishop total-field data set (with magnetic inclination of 90°) their multiwindow Werner deconvolution, interpreting their results on the basis of a number of 'basement indicators,' that is, special grouping of the solutions that, in the authors' experience, can be used to identify the basement depth. Errors vary from about –1.5 to about 0.9 km with an average of about ±0.9 km.

With respect to many of the cited methods, our multiscale approach dealt with solutions selected on the base of their reliability by using the Ridge consistency criterion. This means that, our reconstructed basement map is not defined by a redundant set of estimates, obtained at every point of the data matrix. Our analysis is, instead, focused to special points of the magnetic field, which are related to its singular points. For example, these special points correspond to the extrema of the anomaly in the case of a dipolar source (Fig. 7) or to the anomaly flanks when fault-like sources occur (Fig. 10). Hence, our basin reconstruction is controlled at a set of selected key points, whose number is less than with other methods. For instance, to reconstruct the basement bathymetry, we used results coming from the analysis of about 100 profiles across the Bishop model total-field map, providing 172 depth and N estimates, whereas methods based on a moving window approach, such as the Euler deconvolution, would have obtained a redundant set of solutions virtually equal to the number of data (about 3800 000). These many solutions must be later filtered by efficient algorithms, to separate spurious from valid solutions.

Hence, our approach is certainly less automated than these methods; on the other hand, it does not need any post-processing phase and does not provide ambiguous clusters of solutions, often scattered by some kilometres in the horizontal or vertical directions.

Generally, multiscale methods are used to interpret potential field along selected profiles orthogonal to a 2-D geological structure (Boukerbout & Gibert 2006). Florio *et al*. (2004) showed that results of Euler deconvolution, CWT method or other multiscale approaches are flawed if the vertical differentiation or the upward continuation involved in these methods are computed along a generic profile instead of on a map, unless if the profile crosses normally an elongated anomaly. In our case, the original data, known on a surface, are differentiated and continued to several levels in such a way to form a 3-D data volume. Vertical sections may be easily extracted along any specific direction, thus, taking into account preferential anomaly strike directions.

In this paper, however, to reconstruct the Bishop basement depth map from the magnetic data, the profiles to be analysed were simply extracted along rows and columns of the data matrix, regardless the anomaly strike. This was necessary to perform the process in some automated way.

Ridges are formed on the selected sections, even though they should be more rigorously identified by considering the complete 3-D, conic nature of these structures, as shown in Fedi *et al*. (2010). However, this would imply a not-so-simple visualization of the whole cone, and a preliminary analysis showed that the differences between the two approaches (2-D or 3-D ridge visualization), in terms of parameters estimation, are mostly small.

The estimated depths are presented in Fig. 12, showing a good agreement between the estimated depths (coloured dots) and the true depth to the Bishop basement (filled contours). The depth estimations were obtained at locations corresponding to all the intrabasement magnetization contrasts and along some of the main

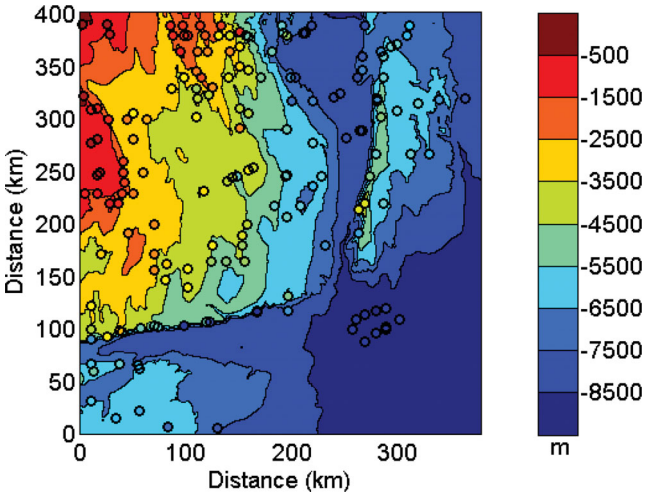

Figure 12. Application of the multiscale approach to the Bishop basement model. Coloured dots represent depth solutions (see the colour bar) and the filled contours represent the basement bathymetry by using the same colour map.

structural features of the basement, such as the steepest sides of the two large-offset main faults. In the southeastern area, the basement top is quite smooth and deep (8–9 km) so that the only notable total-field feature is the strong isolated anomaly caused by a basement intrusion. Thus, in this area, we obtained depth estimations only for this last anomaly. A comparison of the estimated depths with the true depth is presented in Fig. 13, where it can be appreciated how the found depths are, on average, very close to the 45° dashed line, where perfect solutions lie. In Fig. 13, it is also clear how the depth error increases with the anomaly source depth.

However, it can be noted how in some cases (e.g. $x = 140$ km, $y = 290$ km), the depth estimations do not agree well with the true basement depth. It is evident that, in these cases, our strategy to separate the magnetic anomalies generated by the basement morphology and by the magnetized intrusions was unsuccessful.

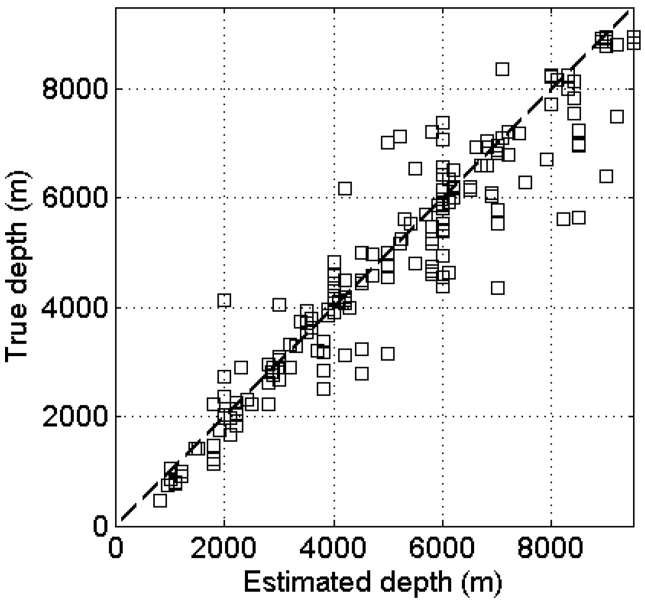

Figure 13. Plot of true depth versus estimated depths for the solutions shown in Fig. 12. Depth solutions with no error lie on the dashed line.

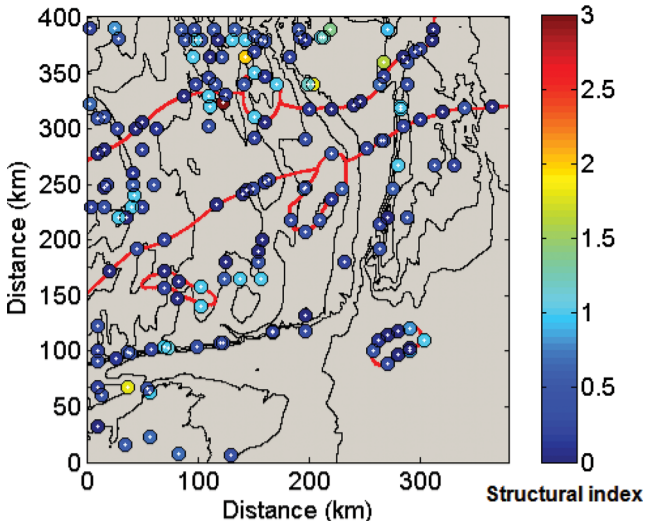

Figure 14. The obtained structural index solutions, selected on the base of their reliability by using the ridge consistency criterion. Coloured dots represent structural index solutions (see the colour bar), the red lines represent the horizontal, intrabasement susceptibility boundaries and the black isolines represent the basement bathymetry.

Generally, we noted a good agreement among the structural index estimations (Fig. 14) and the values expected by considering the structure geometries. The best N estimations were obtained along the susceptibility boundaries between differently magnetized basement blocks or related to the intrusive bodies. In all these cases, we expect N close to 0 (semi-infinite magnetic contacts). The achieved results confirm the contact model for these structures, even if we obtained N values significantly higher than zero close to the structure corners. This is because in those zones, the true structure shape is significantly different from the ideal contact (e.g. the solutions relative to the southeastern intrusive). Although most of the estimated structural indices range from 0 to 1 (Fig. 15), agreeing with the analysis performed by Williams *et al*. (2005), the N solutions histogram shows clear peaks in correspondence of the integers 0 and 1. This histogram feature confirms that differentiation is effective in reducing the interference with nearby sources producing anomalies similar to those expected from ideal sources. Higher structural indices ($1 < N < 2$) are sometimes found in correspondence with complex basement topography (e.g. small ridges) or as a consequence of interference.

Finally, we obtained an image of the recovered basement depth, by interpolating through the whole set of depth estimates (Fig. 16). Comparing Figs 12 and 16, one can see that the main topographic features are well imaged in the map obtained from the estimated depths. The main discrepancies occur in areas where there is a lack of estimates. These areas are associated with low total-field

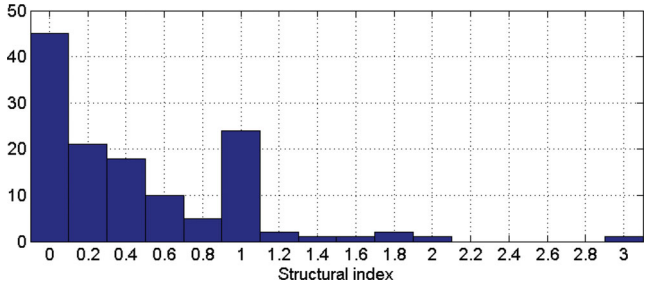

Figure 15. Histogram of the estimated structural indices.

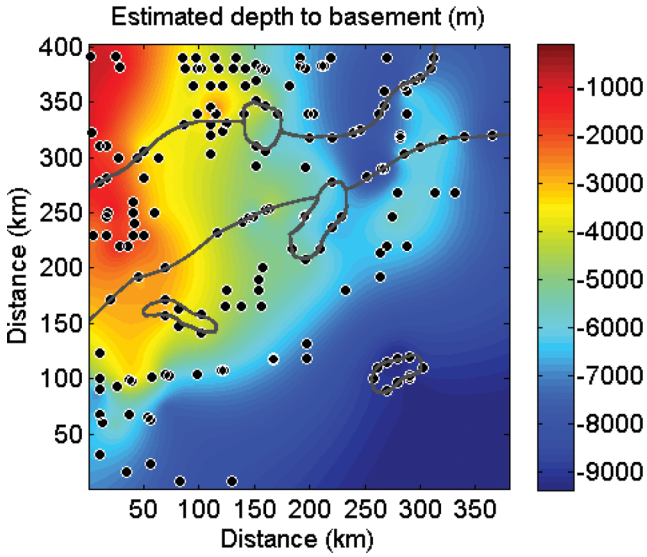

Figure 16. Recovered basement depth, interpolated from the obtained depth estimates (black dots). The grey lines represent the horizontal, intrabasement susceptibility boundaries.

horizontal gradients, such as, at the flat bottom of the east–west and north–south canyons and along the less steep sides of the same canyons. In these conditions, the interpreted field has low amplitude and the ridges have a low inclination: These factors do not allow a good ridge development.

5 CONCLUSIONS

In this paper, we propose a new approach to analyse potential fields by estimating source parameters, such as, the horizontal position and depth of simple equivalent sources and the structural index N, representing the source type. This approach includes estimations of the depth to source, performed with the multiscale geometrical method, and of the structural index, achieved by ScalFun method. The key points are:

1. The introduction of a new criterion, the ridge consistency criterion, to evaluate the validity of the source parameters estimations. This criterion is based on the computation of field derivatives to reduce anomaly coalescence as well as the influence of regional fields. We verified the effectiveness of this approach with tests on magnetic data, but we expect that this method should be even more effective and necessary for gravity data, because in that case the coalescence effects are more pronounced than in magnetic data.
2. The reconstruction of a complex basement, such as the Bishop model, is not made using a redundant set of estimates, such as the methods based on a 'moving window' approach, but with a reduced set of the estimates on key anomalies.

We applied our multiscale approach to the magnetic field generated by the Bishop complex basement model. According to our theory, a relatively low number of analysed profiles were enough to obtain a rather accurate map of the basement relief. Also, the structural index estimates were in good agreement with the structure morphology of the basement.

In this paper, we also showed that it is possible to build a reliable multiscale data set by applying the upward-continuation operator to the measured data set. After testing several extrapolation algorithms, accurate upward-continued fields were provided, when a reasonable extension algorithm is used and the field is horizontally extended

over an area large enough to circumvent aliasing from circular convolution.

We also showed that field measurements at two different altitudes, as a minimum, can be enough to check the quality of the upward continuation and allowing the construction of a reliable 3-D data set even at very high altitudes/sampling-step ratios.

ACKNOWLEDGMENTS

The authors sincerely thank the reviewers, Dr M.F. Mushayandebvu, for the many useful corrections and observations, and Prof D. Gibert, for his constructive comments. The Associate Editor and the reviewers helped us to substantially improve our original manuscript.

REFERENCES

Boukerbout, H. & Gibert, D., 2006. Identification of sources of potential fields with the continuous wavelet transform: Two-dimensional ridgelet analysis, *J. geophys. Res.,* **111,** B07104, doi:10.1029/2005JB004078.

Fedi, M., 2007. DEXP: a fast method to determine the depth and the structural index of potential fields sources, *Geophysics,* **72**(1), I1–I11, doi:10.1190/1.2399452.

Fedi, M., Cella, F., Quarta, T. & Villani, A., 2010. 2D Continuous wavelet transform of potential fields due to extended source distributions, *Appl. Comput. Harmon. Anal.,* **28**(3), 320–337.

Fedi, M. & Florio, G., 2006. SCALFUN: 3D analysis of potential field scaling function to determine independently or simultaneously Structural Index and depth to source, *SEG Expanded Abstract,* **25,** 963–967, doi:10.1190/1.2372499.

Fedi, M., Florio, G. & Quarta, T., 2009. Multiridge analysis of potential fields: geometrical method and reduced Euler deconvolution, *Geophysics,* **74**(4), L53–L65

Florio, G. & Fedi, M., 2006. Euler deconvolution of vertical profiles of potential field data, *SEG Expanded Abstracts,* **25,** 958–962, doi:10.1190/1.2370415.

Florio, G. & Fedi, M., 2009. Euler deconvolution for a multiridge set, in *71st EAGE Conference & Exhibition,* Extended Abstract, p. T042, http://www.earthdoc.org/detail.php?pubid=24031.

Florio, G., Fedi, M. & Cella, F., 2004. On the use of two- vs. three- dimensional transformation and interpretation of potential field anomalies, in *Proceedings of the Near Surface 2004—10th European Meeting of Environmental and Engineering Geophysics,* Utrecht, the Netherlands, pp. P011.

Florio, G., Fedi, M. & Rapolla, A., 2009. Interpretation of regional aeromagnetic data by multiscale methods: the case of Southern Apennines (Italy), *Geophys. Prospect.,* **57,** 479–489.

Gibert, D. & Galdéano, A., 1985. A computer program to perform transformations of gravimetric and aeromagnetic surveys, *Comput. Geosci.,* **11,** 553–588.

Goussev, S.A. & Pierce, J.W., 2010. Magnetic basement: gravity-guided magnetic source depth analysis and interpretation, *Geophys. Prospect.,* **58,** 321–334.

Mallat, S., 1998. *A Wavelet Tour of Signal Processing,* Academic Press, San Diego, CA.

McGrath, P.H., 1991. Zero crossover—a FORTRAN program to determine the dip and extent of a geological boundary using horizontal derivatives of upward continued gravity data, *Comput. Geosci.,* **17**(7), 1017–1032.

Moreau, F., Gibert, D., Holschneider, M. & Saracco, G., 1997. Wavelet analysis of potential fields, *Inverse Probl.,* **13,** 165–178.

Oppenheim, A.V. & Schafer, R.W., 1975. *Digital Signal Processing,* Prentice-Hall, Englewood Cliffs, NJ.

Paul, M.K., Datta, S. & Banerjee, B., 1966. Direct interpretation of two-dimensional structural faults from gravity data, *Geophysics,* **31,** 940–948.

Paul, M.K. & Goodacre, A.K., 1984. The gravity profile and its role in positioning the edge of a two-dimensional faulted structure having an arbitrary vertical variation of density, *Geophysics,* **49,** 1097–1104.

Pedersen, L.B., 1991. Relations between potential fields and some equivalent sources, *Geophysics,* **56,** 961–971.

Reid, A., FitzGerald, D. & Flanagan, G., 2005. Hybrid Euler magnetic basement depth estimation: Bishop 3D tests, *SEG Expanded Abstracts,* **24,** 671–673, doi:10.1190/1.2144412.

Sailhac, P. & Gibert, D., 2003. Identification of sources of potential fields with the continuous wavelet transform: two dimensional wavelets and multipolar approximations, *J. geophys. Res.,* **108**(B5), 2262, doi:10.1029/2002JB002021.

Salem A., Williams, S., Fairhead, D., Smith, R. & Ravat, D., 2008. Interpretation of magnetic data using tilt-angle derivatives, *Geophysics,* **73**(1), L1–L10.

Stavrev, P. & Reid, A., 2007. Degrees of homogeneity of potential fields and structural indices of Euler deconvolution, *Geophysics,* **72**(1), L1–L12.

Steenland, N.C., 1968. On: "The geomagnetic gradiometer" by H. A. Slack, V. M. Lynch, and L. Langan (GEOPHYSICS, October 1967, p. 877–892). *Geophysics,* **33,** 680–683.

Williams, S., Fairhead, J.D. & Flanagan, G., 2002. Realistic models of basement topography for depth to magnetic basement testing, *SEG Expanded Abstracts,* **21,** 814–817, doi:10.1190/1.1817384.

Williams, S., Fairhead, J.D. & Flanagan, G., 2005. Comparison of grid Euler deconvolution with and without 2D constraints using a realistic 3D magnetic basement model, *Geophysics,* **70**(3), L13–L21.